

Article

Numerical Study of Local Scour around Tripod Foundation in Random Waves

Ruigeng Hu ¹, Xiuhai Wang ^{1,2,3,*}, Hongjun Liu ^{1,2,3} and Da Chen ¹

¹ College of Environmental Science and Engineering, Ocean University of China, Qingdao 266005, China; huruigeng@stu.ouc.edu.cn (R.H.); hongjun@ouc.edu.cn (H.L.); 21191011084@stu.ouc.edu.cn (D.C.)

² Key Laboratory of Marine Environment and Ecology, Ocean University of China, Ministry of Education, Qingdao 266005, China

³ Key Laboratory of Shandong Province for Marine Environment and Geological Engineering, Ocean University of China, Qingdao 266005, China

* Correspondence: showseas@ouc.edu.cn

Abstract: In this study, the local scour around tripods in random waves is numerically investigated. The seabed-tripod-fluid numerical model with an RNG $k-\varepsilon$ turbulence model is built and validated. Following that, the scour characteristics and flow velocity distribution are analyzed using the present numerical model. Finally, a revised stochastic model is proposed to predict the equilibrium scour depth, S_{eq} , around tripods in random waves. The results indicate that the present seabed-tripod-fluid numerical model is capable of depicting the scour process and of capturing the flow field around tripods with high accuracy. Due to the blockage effects of the main column and structural elements, there is enhanced flow acceleration underneath the main column and the lower diagonal braces, which increases the turbulence intensity and seabed shear stress, causing more particles to be mobilized and transported, resulting in more severe scour at the site. The revised stochastic model shows the best agreement with the numerical and experimental results when $n = 20$, but more experimental data and numerical results are still needed to verify the adaptation of the revised stochastic model for larger Keulegan–Carpenter (KC) number conditions ($KC_{rms,a} > 4$).

Keywords: scour; tripod foundation; equilibrium scour depth; KC number; numerical simulation



Citation: Hu, R.; Wang, X.; Liu, H.; Chen, D. Numerical Study of Local Scour around Tripod Foundation in Random Waves. *J. Mar. Sci. Eng.* **2022**, *10*, 475. <https://doi.org/10.3390/jmse10040475>

Academic Editor: Kamal Djidjeli

Received: 22 February 2022

Accepted: 26 March 2022

Published: 29 March 2022

Publisher's Note: MDPI stays neutral with regard to jurisdictional claims in published maps and institutional affiliations.



Copyright: © 2022 by the authors. Licensee MDPI, Basel, Switzerland. This article is an open access article distributed under the terms and conditions of the Creative Commons Attribution (CC BY) license (<https://creativecommons.org/licenses/by/4.0/>).

1. Introduction

Offshore wind energy is a type of clean and renewable energy, and it has developed rapidly in recent decades. There are many variations in foundation types for offshore wind turbines (OWTs), such as monopile, suction anchor (or bucket), gravity foundation, jacket, and tripod [1,2]. To date, the monopile type has been widely adopted in offshore wind farms when the water depth is less than 30 m [3]. For the deep water zone, the tripod foundation is a feasible plan for OWTs with favorable bearing capacity and stability [3–6]. When a foundation is installed in a seabed, it is exposed to waves and currents in all life cycles. The flow field is affected by the presence of the foundation, leading to a horseshoe vortex, flow acceleration, and vortex shedding in the vicinity of the foundation [7–9]. As a result, enhanced mobility in soil particles develops, and consequently, local scour holes emerge around the foundation. As scour holes develop, the embedded depth of the foundation decreases, which weakens the stability and durability of the foundation and even results in a complete collapse of the supporting system [10–13]. Therefore, scour development and scour depth prediction around a foundation are important for OWT design.

A considerable number of studies revealed that the horseshoe vortex, flow acceleration, and wake vortex shedding are mainly responsible for scour around a single pile [7,9,14–16]. The scour evolution and scour topography in waves are significantly and simultaneously affected by the Keulegan–Carpenter (KC) number and the Shields parameter θ [17–19]. Compared with θ , the KC number exerts considerably more influence on scour topography [9,17,18].

Based on the wave flume scour tests for a single pile conducted by Sumer et al. [14,15], the lifespan and intensity of a horseshoe vortex obviously increases with an increase in KC , so higher KC results in a greater equilibrium scour depth S_{eq} . Hassan et al. [20,21] developed a novel gene expression program and artificial neural networks to predict the local scour depth around a bridge pier. Welzel et al. [22,23] carried out a series of laboratory scour tests to study scour evolution around a jacket foundation in combined waves and currents, concluding that significant flow acceleration in the vicinity of diagonal braces contributes to the enhanced mobility of soil particles and, consequently, a greater scour depth. Compared with a single pile, the tripod foundation has complex shapes, and it comprises one main column, three monopiles, and some diagonal braces connecting monopiles and the main column. The flow field varies with the shape of the foundation, so the shape may have an obvious influence on scour development and scour depth [24]. Therefore, the results about scour development and scour depth prediction from a single pile cannot be directly applied for foundations with complex shapes.

Stahlmann [3] carried out a series of field surveys to monitor scour depth around a tripod, finding that the maximum scour depth occurs underneath the main column. Several groups of flume tests were conducted to investigate scour development and the scour characteristics around a tripod under random waves, and the results indicate that the scour depths increase quickly at the initial stage, followed by slower growth until the equilibrium stage is reached. For all experiments, the location of the maximum scour depth is situated beneath the main column. The scour evolution and scour depth around a tripod under collinear waves and currents were numerically studied by Yamini et al. [5]. The calculated results reveal that the higher the wave height, the greater the flow velocity, with finer sediment granularity resulting in a larger equilibrium scour depth. Yuan et al. [4] investigated the scour characteristic and scour mechanism around a tripod foundation in steady currents using laboratory flume tests, and the results indicated that the scour holes emerged both around the tripod piles and beneath the main column. These scour holes extended along the lower diagonal braces, and the maximum scour depth ($S_{max} = 3.5 D$, with D being the diameter of the main column) occurred in the vicinity of the tripod's downstream pile. Notably, the maximum scour depth amounts to three times the design value recommended by the Offshore Standard [25] for a single pile. Based on these data, it can be asserted that the tripod may lead to the seabed suffering from more severe scour than a single pile.

So far, compared with research about the scour around monopiles, very few experimental and numerical studies are available for the scour around tripods and the formulas for predicting the equilibrium scour depth S_{eq} around tripod are also limited. In this way, the scour design approach for tripods is generally provided based on the criteria of monopiles, which may lead to an underestimation in the level of scour damage. As a result, it can cause considerable safety risks for the offshore wind turbine. Given that, in this study, the scour characteristics and equilibrium scour depth around tripods in random waves were numerically investigated. This paper is organized as follows. Firstly, the seabed-tripod-fluid numerical model with an $RNG k-\epsilon$ turbulence model is built and validated. After that, the scour characteristics and flow velocity distribution are analyzed using the present numerical model. Finally, a revised stochastic model is proposed to predict the equilibrium scour depth around a tripod in random waves.

2. Numerical Model

2.1. Momentum Equations

The following three equations (RANS equations) are used to describe the incompressible viscous fluid motion [26]:

$$\frac{\partial u}{\partial t} + \frac{1}{V_F} (u A_x \frac{\partial u}{\partial x} + v A_y \frac{\partial u}{\partial y} + w A_z \frac{\partial u}{\partial z}) = -\frac{1}{\rho} \frac{\partial p}{\partial x} + G_x + f_x \quad (1)$$

$$\frac{\partial v}{\partial t} + \frac{1}{V_F} (uA_x \frac{\partial v}{\partial x} + vA_y \frac{\partial v}{\partial y} + wA_z \frac{\partial v}{\partial z}) = -\frac{1}{\rho} \frac{\partial p}{\partial y} + G_y + f_y \tag{2}$$

$$\frac{\partial w}{\partial t} + \frac{1}{V_F} (uA_x \frac{\partial w}{\partial x} + vA_y \frac{\partial w}{\partial y} + wA_z \frac{\partial w}{\partial z}) = -\frac{1}{\rho} \frac{\partial p}{\partial z} + G_z + f_z \tag{3}$$

where $u, v,$ and w are the flow velocity components in $x, y,$ and z directions, respectively; V_F is the volume fraction; A_i ($i = x, y, z$) is the area fraction; ρ_f is the water density; f_i is the viscous force; and G_i is the body force.

2.2. Turbulence Model

The momentum equations can be solved using a combination of turbulence models. The RNG $k-\epsilon$ model is a two-equation turbulence model, and it can compute the near-wall flow field accurately with high efficiency [26,27]. Therefore, the RNG $k-\epsilon$ model was employed to capture the flow field around tripods.

$$\frac{\partial k_T}{\partial T} + \frac{1}{V_F} (uA_x \frac{\partial k_T}{\partial x} + vA_y \frac{\partial k_T}{\partial y} + wA_z \frac{\partial k_T}{\partial z}) = P_T + G_T + Diff_{k_T} - \epsilon_{k_T} \tag{4}$$

$$\frac{\partial \epsilon_T}{\partial T} + \frac{1}{V_F} (uA_x \frac{\partial \epsilon_T}{\partial x} + vA_y \frac{\partial \epsilon_T}{\partial y} + wA_z \frac{\partial \epsilon_T}{\partial z}) = \frac{CDIS1\epsilon_T}{k_T} (P_T + CDIS3G_T) + Diff_{\epsilon_T} - \frac{CDIS2\epsilon_T^2}{k_T} \tag{5}$$

where k_T is the kinetic energy associated with turbulent velocity; P_T is the turbulent kinetic energy; ϵ_T is the turbulent energy dissipating rate; G_T is the turbulent energy generated by buoyancy; $Diff_{\epsilon}$ and $Diff_{k_T}$ are diffusion terms; and $CDIS1, CDIS2,$ and $CDIS3$ are dimensionless parameters, where $CDIS1$ and $CDIS3$ have default values of 1.42 and 0.2, respectively, and $CDIS2$ can be acquired using P_T and k_T .

2.3. Sediment Scour Model

2.3.1. Entrainment and Deposition

The entrainment lift velocity of particles can be obtained from Equation (6) [28].

$$u_{lift,i} = \alpha_i n_s d_*^{0.3} (\theta - \theta_{cr})^{1.5} \sqrt{\frac{\|g\| d_i (\rho_i - \rho_f)}{\rho_f}} \tag{6}$$

where α_i is the entrainment parameter, n_s is the normal vector perpendicular to the seabed and $n_s = (0,0,1)$ for the present numerical model, θ_{cr} is the critical Shields parameter, g is the gravity acceleration, d_i is the diameter of particles, ρ_i is the density of bed species, and d_* is the dimensionless diameter of particles and can be obtained from Equation (7).

$$d_* = d_i \left(\frac{\|g\| \rho_f (\rho_i - \rho_f)}{\mu_f^2} \right)^{1/3} \tag{7}$$

where μ_f is the fluid dynamic viscosity.

Based on Soulsby [29], θ_{cr} was calculated from Equation (8).

$$\theta_{cr} = \frac{0.3}{1 + 1.2d_*} + 0.055 [1 - \exp(-0.02d_*)] \tag{8}$$

The settling velocity of sand particles was computed from Equation (9) [29]

$$\mathbf{u}_{settling,i} = \frac{\nu_f}{d_i} \left[(10.36^2 + 1.049d_*^3)^{0.5} - 10.36 \right] \tag{9}$$

where ν_f is the fluid kinematic viscosity.

2.3.2. Bed Load Transportation

According to Van Rijn [30], the bed load transportation velocity was calculated as

$$u_{bedload,i} = \frac{q_{b,i}}{\delta_i c_{b,i} f_b} \tag{10}$$

where $q_{b,i}$ is the bed load transportation rate and can be acquired using Equation (11), δ_i is the bed load thickness and can be obtained from Equation (12), f_b is the critical packing fraction of the particles, and $c_{b,i}$ is the volume fraction of sand i .

$$q_{b,i} = 8 \left[\|g\| \left(\frac{\rho_i - \rho_f}{\rho_f} \right) d_i^3 \right]^{1/2} \tag{11}$$

$$\delta_i = 0.3 d_*^{0.7} \left(\frac{\theta}{\theta_{cr}} - 1 \right)^{0.5} d_i \tag{12}$$

2.3.3. Suspended Load Transportation

The suspended sand concentration was calculated using the following equations.

$$\frac{\partial C_{s,i}}{\partial t} + \nabla(\mathbf{u}_{s,i} C_{s,i}) = \nabla \nabla (D_f C_{s,i}) \tag{13}$$

where $C_{s,i}$ is the suspended particles mass concentration of sand i , $\mathbf{u}_{s,i}$ is the particles velocity of sand i , and D_f is the diffusivity.

The $\mathbf{u}_{s,i}$ can be calculated using the following equation:

$$\mathbf{u}_{s,i} = \bar{\mathbf{u}} + \mathbf{u}_{setting,i} C_{s,i} \tag{14}$$

where $\bar{\mathbf{u}}$ is the velocity of mixed fluid-particles and can be obtained using a combination of the RANS equations and the turbulence model, and $c_{s,i}$ is the suspended particles volume concentration and can be computed from Equation (15).

$$c_{s,i} = \frac{C_{s,i}}{\rho_i} \tag{15}$$

3. Model Setup

The seabed-tripod-fluid numerical model (shown in Figure 1) was built to study scour characteristics around tripods in random waves. The model was made up of a seabed, the tripod foundation, as well as fluid and porous media. The dimensions of the seabed were 240 m × 40 m × 3 m (length × width × height), which consisted of uniform fine sand with median diameters of $d_{50} = 0.051$ cm. The diameter of main column D was 2.5 m. The bottom of the main column was a distance of $3D$ from the initial seabed. The tripod was located at the center of the seabed, with a distance of 140 m from the offshore side and 100 m from the onshore side. The porous media were placed on the onshore side above the seabed to eliminate wave reflection.

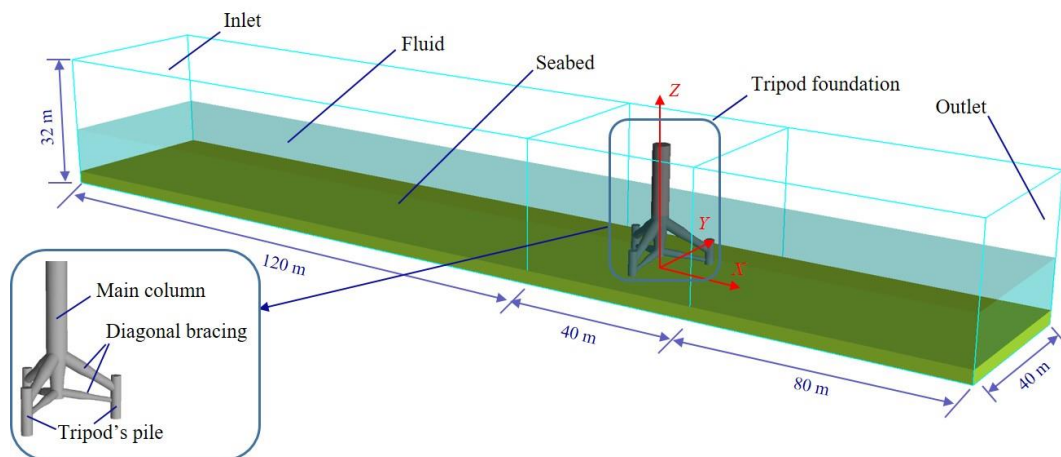


Figure 1. A sketch of the seabed-tripod-fluid numerical model.

3.1. Mesh Generation

The mesh grid of the model is shown in Figure 2. Two types of meshes (global mesh and nested mesh grid) were used in the present model. The dimensions of the whole mesh grid were 240 m × 40 m × 32 m (length × width × height), which was generated by the hexahedral global mesh grid. In order to improve the mesh quality and the calculation accuracy, a finer nested mesh grid was generated around the tripod from −20 to 20 in the *x* direction, from −20 to 20 in the *y* direction, and from 0 to 32 m in the *z* direction. The detailed process of confirming the adaptable mesh size is described in the following Mesh Sensitivity section.

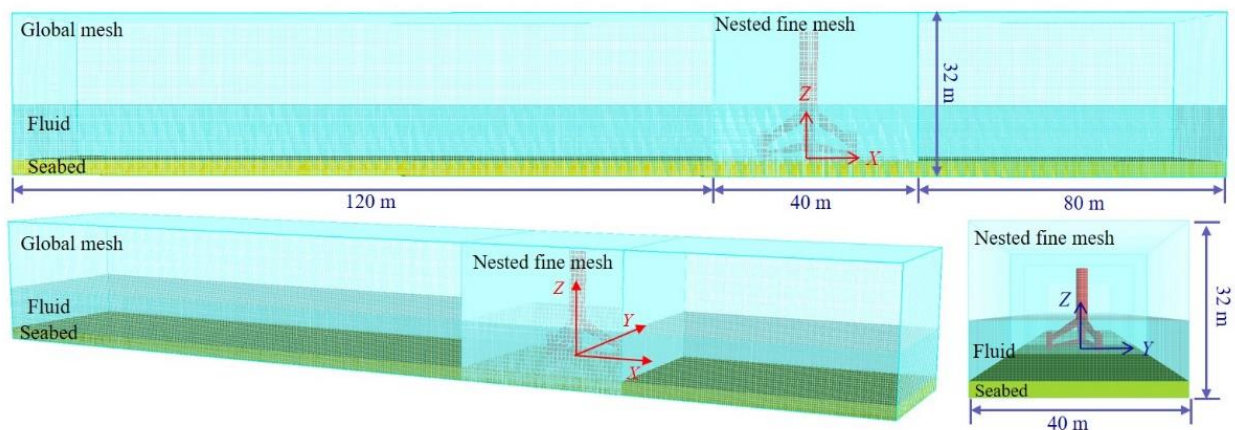


Figure 2. A sketch of the mesh block.

3.2. Boundary Conditions

Two sides of the model in the *x*-*z* plane and the top side were defined as the symmetry boundaries because it is an advisable approach to improving calculation efficiency. The wall boundary at the bottom was selected so that $u = v = w = 0$. The wave boundary was set at the upstream offshore end. For wave boundary, the Joint North Sea Wave Project (JONSWAP) wave spectrum was adopted to generate random waves. Based on Yu and Liu [31], the unidirectional JONSWAP frequency spectrum can be expressed by

$$S(\omega) = \frac{\alpha g^2}{\omega^5} \exp\left[-\frac{5}{4}\left(\frac{\omega_p}{\omega}\right)^4\right] \gamma \exp\left[-\frac{(\omega - \omega_p)^2}{2\sigma^2 \omega_p^2}\right] \quad (16)$$

where α is the wave energy scale parameter and can be acquired from Equation (17); ω is the frequency; ω_p is the wave spectrum peak frequency and can be calculated using

Equation (18); σ is the spectral width factor, where $\sigma = 0.07$ when $\omega \leq \omega_p$ and $\sigma = 0.09$ when $\omega > \omega_p$; and γ is the wave spectrum peak enhancement factor ($\gamma = 3.3$ for this study).

$$\alpha = 0.0076 \left(\frac{gX}{U^2} \right)^{-0.22} \tag{17}$$

$$\omega_p = 22 \left(\frac{g}{U} \right) \left(\frac{gX}{U^2} \right)^{-0.33} \tag{18}$$

where X is the fetch length and U is the average wind velocity at a height of 10 m from the mean water table.

For the JONSWAP wave spectrum, the input parameters include X and U , and the combination of X and U can generate the needed wave heights and wave periods. The wave parameters are listed in Table 1. Eleven groups of numerical models were calculated to study the scour characteristics around tripods in random waves.

Table 1. Test plans and numerical parameters.

No.	d (m)	$H_{1/3}$ (m)	T_P (s)	$U_{wm,rms}$ (m/s)	$KC_{rms,a}$	S_{eq}/D
1	8	2.5	9.53	0.769	2.211	0.201
2	8	3.0	10.37	0.961	3.006	0.245
3	8	3.5	10.76	1.141	3.702	0.266
4	9	3.0	10.37	0.883	2.762	0.225
5	9	3.5	10.76	1.050	3.407	0.250
6	10	3.0	10.37	0.814	2.545	0.201
7	10	3.5	10.76	0.971	3.151	0.248
8	11	3.0	10.37	0.854	2.671	0.192
9	11	3.5	10.76	0.902	2.927	0.238
10	12	3.0	10.37	0.700	2.189	0.183
11	12	3.5	10.76	0.839	2.722	0.211

3.3. Mesh Sensitivity

The calculated results show close correlation with mesh resolution; therefore, mesh sensitivity analysis is vital before making further investigations about scour characteristics and scour depth prediction. In this section, four types of mesh grid sizes were chosen: Mesh 1—global mesh size of 0.3×0.3 and nested fine mesh size of 0.2×0.2 , Mesh 2—global mesh size of 0.2×0.2 and nested fine mesh size of 0.1×0.1 , Mesh 3—global mesh size of 0.15×0.15 and nested fine mesh size of 0.05×0.05 , and Mesh 4—global mesh size of 0.1×0.1 and nested fine mesh size of 0.03×0.03 . The numerical parameters are the same as case 8 in Table 1. The calculated scour hole profiles around the tripod with the range of -4 – 4 m in the x direction were compared under four mesh sizes, and the results at scour duration $t = 3600$ s are displayed in Figure 3. As the Figure 3 indicates, compared with the relative coarse mesh size (e.g., Mesh 1), a finer mesh size (e.g., Mesh 3 or Mesh 4) results in a greater scour depth, indicating that a finer mesh size can capture the flow field and scour process around a tripod with high accuracy. Notably, a finer mesh size needs huger time costs and higher computer configuration. As displayed in Figure 3, the maximum error in the scour depth between Mesh 3 and Mesh 4 is about 3.2 %. Based on the mesh sensitivity guideline used by Pang et al. [32], it can be asserted that the results converged and that the mesh size is independent when Mesh 3 is adopted. In this way, to ensure accurate calculations and to save on computation time, Mesh 3 was used to calculate the scour process around the tripod in the following sections.

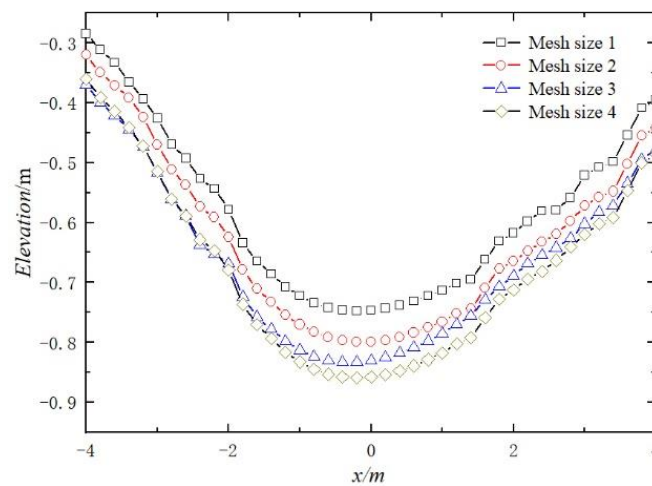


Figure 3. Comparison of the scour hole profiles with different mesh grid sizes.

3.4. Model Validation

To validate the adaptation and accuracy of the present numerical model, comparisons between the calculated results from the present model and the experimental results from Sumer and Fredsøe [7], and Schendel et al. [33] were conducted. Figure 4 displays the experimental results of Run01, Run05, Run21, and Run22 from Sumer and Fredsøe [7]; the experimental results of A05 and A09 from Schendel et al. [33]; and the numerical results from the present model. Based on Figure 4, the maximum error between the numerical results and experimental data is about 30%, which indicates that the numerical results show an overall agreement with the experimental data, demonstrating that the present numerical model can capture the scour process precisely and can predict the equilibrium scour depth or maximum scour depth around foundations with high accuracy.

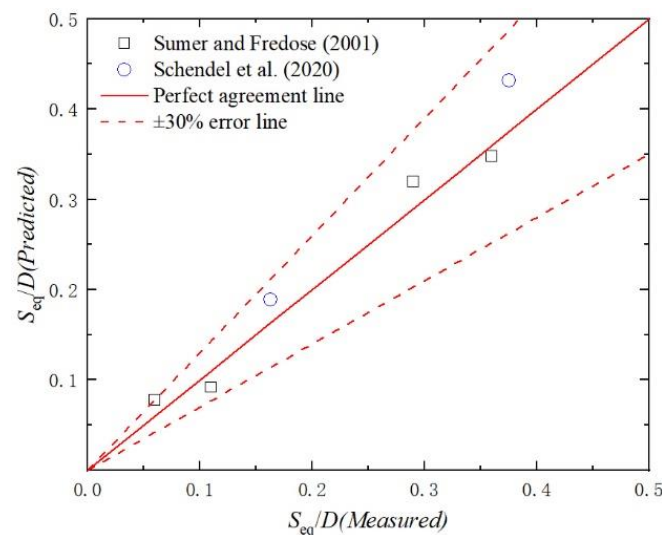


Figure 4. Comparison of the maximum or equilibrium scour depth between the present study and Sumer and Fredsøe [7], and Schendel et al. [33].

4. Numerical Results

4.1. Scour Evolution

Figure 5 depicts the temporal development of scour underneath the main column for cases 1, 3, and 4. As the Figure 5 indicates, the scour holes developed rapidly during the first 0–1000 s, and after that, the scour rate decreased. After approximately 3000 s, the scour depths gradually stabilized and attained an asymptotic value. Equation (19) proposed by

Sumer and Fredsøe [7] was adopted to fit the experimental data, and the results indicate that Equation (19) is capable of depicting the scour process accurately around tripod in random waves.

$$S_t = S_{eq}(1 - \exp(-t/T_c)) \tag{19}$$

where T_c is the scour time scale.

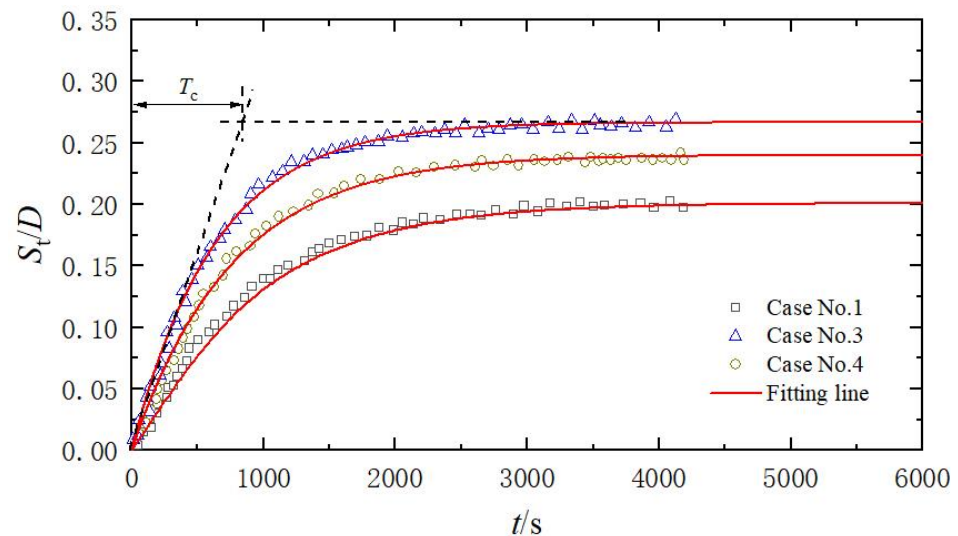


Figure 5. Temporal development of scour underneath the main column for cases 1, 3, and 4.

The scour evolution curves kept fluctuating significantly when $t = 4000$ s, so it can be concluded that the scour did not attain equilibrium based on the equilibrium guidelines suggested by Melville and Chew [34]. Therefore, the equilibrium scour depth, S_{eq} , was obtained using the fitting approach and Equation (19), and the S_{eq} are listed in Table 1.

4.2. Scour Characteristics and Flow Velocity Distribution

Figure 6 shows a sequence of scour morphologies around the tripod for case 3. As Figure 6 indicates, at the initial stage ($t = 600$ s), the scour hole appeared beneath the main column and extended along the diagonal braces connected to the wall-facing pile. After that, following approximately 300 wave cycles, the scour topography gradually stabilized; these findings are similar to the experimental results of Sthelman [3] and Yamini et al. [5]. The scour development can be explained by the flow velocity distribution in the x - y section (Figure 7) and the x - z section (Figure 8). As shown in Figures 7 and 8, when the incoming waves attacked the tripod, due to the blockage effects of the main column and structural elements, there was enhanced flow acceleration underneath the main column and the lower diagonal braces. The amplified near-bed flow velocity increases the turbulence intensity and the bed shear stress around tripod, causing more particles to be mobilized and transported, which leads to more severe scour at the site. Overall, compared with a single pile, the tripod’s main column and structural elements exert considerable influence on the flow velocity distribution and, hence, on scour process and scour morphology. Additionally, there is a gap between the main column and seabed, so the gap flow may also facilitate the scour process. According to Stahlmann [3] and Yamini et al. [5], the scour hole appeared beneath the main column first and then extended along the lower structural elements. Given these findings, it seems an advisable choice to anchor the main column in the seabed, and it is worthwhile to further study the scour characteristics for this type of foundation in following studies.

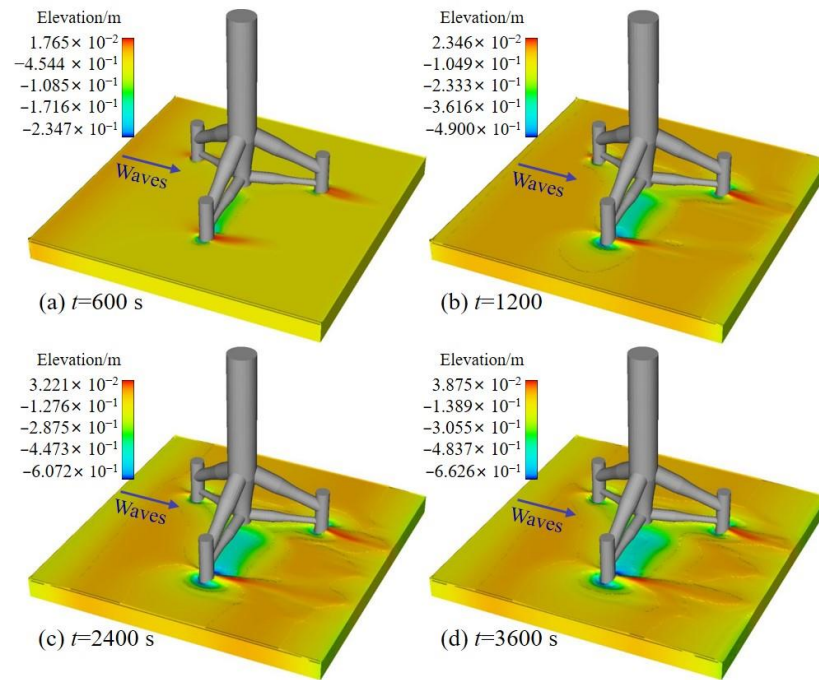


Figure 6. A sequence of scour morphologies around the tripod in case 3.

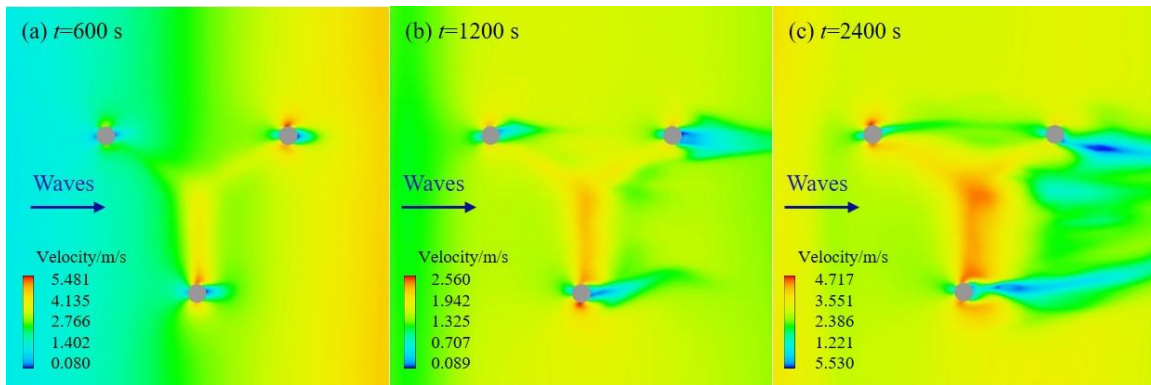


Figure 7. Flow velocity distribution around a tripod in the x - y section.

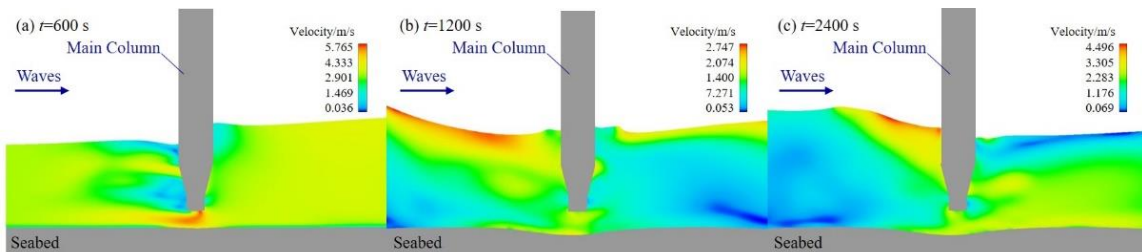


Figure 8. Flow velocity distribution around a tripod in the x - z section.

4.3. Equilibrium Scour Depth Prediction

According to previous studies [7,9,16,35–37], the KC number plays a dominant role in scour processes and scour depths, and a higher KC results in a greater equilibrium scour depth S_{eq} . For random waves, when foundation diameter D is fixed, the different combinations of the wave period T and the maximum near-bed velocity U_{wm} will obtain different KCs . For example, $KC_{rms,a}$ is obtained from the root-mean-square (RMS) value of the maximum near-bed velocity $U_{wm,rms}$ and the average up zero-crossing wave period T_a .

For field conditions, random waves are made up of a sequence of sinusoidal (or cosinoidal) waves with different wave heights and wave periods. Wave heights usually obey a normal distribution, so the wave energy is mainly supplied by the median wave heights. According to Myrhaug and Rue [38], for random waves, the 1/*n*'th highest wave generally dominates the scour process. Based on that, they proposed a stochastic model (Equation (20)) to calculate the *S*_{eq} around a single pile in random waves. In order to validate the adaption of the stochastic model for a tripod foundation, a comparison between the predicted values from the stochastic model and the numerical results from the present study was conducted, and the results are shown in Figure 9.

$$S'_{eq} = 1.3D \left\{ 1 - \exp \left[-0.03(KC_{rms,a}^2 \ln n + 36)^{1/2} - 6 \right] \right\} \quad (20)$$

where *n* denotes the 1/*n*'th highest wave in a sequence of waves.

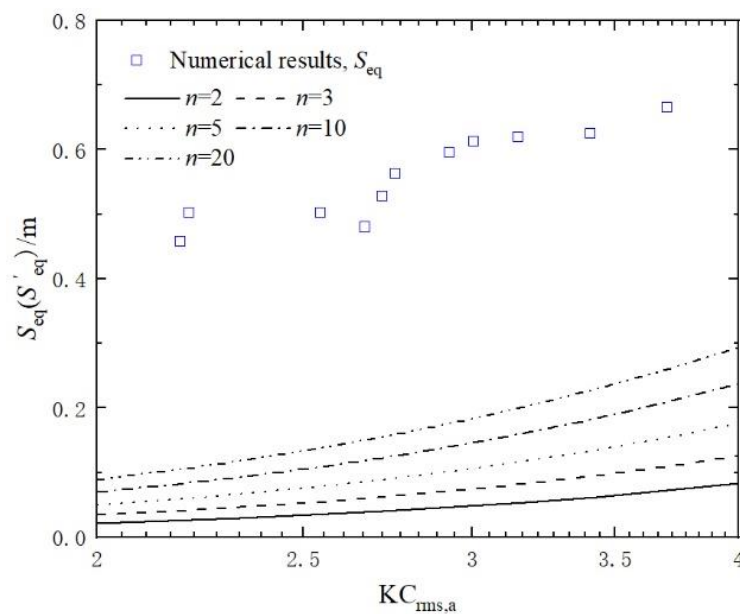


Figure 9. Comparison of *S*_{eq} between the predicting results from the stochastic model and the numerical results of the present study.

As Figure 9 indicates, the stochastic model generally underestimates the *S*_{eq} around tripods, which can be attributed to the stochastic model that was derived based on the experimental results of a single pile. Compared with the case of a single pile, the seabed around tripods suffered from more severe scour due to the blockage effects induced by the structural elements and main column. Notably, although considerable errors exist, the variation rule between the *S*_{eq} and *KC*_{rms,a} predicted by the stochastic model shows favorable agreement with the numerical results of the present study. Therefore, it is feasible to add the deviation value ΔS into the stochastic model to predict the *S*_{eq} around tripods in random waves. Figure 10 gives ΔS for the different *KC*_{rms,a} and plots the fitting line (Equation(21)) between ΔS and *n*. In this way, the revised stochastic model can be obtained by adding $\Delta S/D$ into Equation (20) to predict the *S*_{eq} around tripods in random waves and can be expressed by Equation (22).

$$\Delta S = 0.174 * \exp(-n/6.459) + 0.383 \quad (21)$$

$$S''_{eq} = S'_{eq} + 0.174 * \exp(-n/6.459) + 0.383 \quad (22)$$

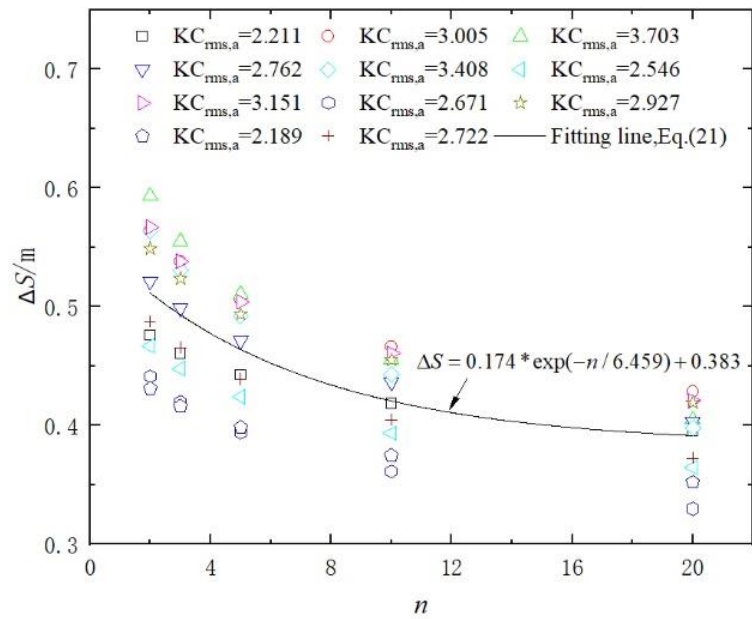


Figure 10. The deviation value ΔS for different $KC_{rms,a}$ and the fitting results between ΔS and n .

Figure 11 shows a comparison between the predicted results from the revised stochastic model and the numerical results of the present study. From Figure 11, it can be seen that the predicted values show the best agreement with the numerical results when $n = 20$, indicating that the revised stochastic model can predict the S_{eq} around tripods in random waves with high accuracy. It is noted that the present numerical model was established based on prototype dimensions with a relatively larger diameter, leading to the scour prevailing under smaller KC conditions. In other words, from Figure 11, the adaptation of the revised stochastic model was only validated for the relatively smaller KC conditions ($KC_{rms,a} < 4$), but more experimental data and numerical results are still needed to verify the adaptation of the revised stochastic model for larger KC conditions ($KC_{rms,a} > 4$).

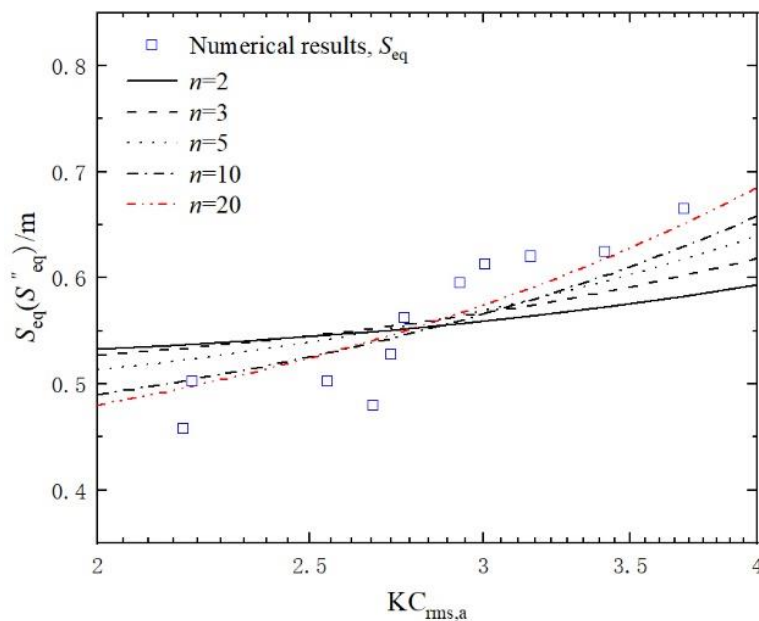


Figure 11. Comparison of S_{eq} between the predicted results from the revised stochastic model and the numerical results of the present study.

5. Conclusions

This study presents numerical data about scour around tripods in random waves. Firstly, the seabed-tripod-fluid numerical model with a RNG $k-\varepsilon$ turbulence model was built and validated. After that, the scour characteristics and flow velocity distribution were analyzed using the present numerical model. Finally, a revised stochastic model was proposed to predict the equilibrium scour depth S_{eq} around tripods in random waves. The main conclusions can be listed as follows.

- (1) The present seabed-tripod-fluid numerical model is capable of depicting the scour process and of capturing the flow field around tripods with high accuracy, indicating that the present seabed-tripod-fluid numerical model is adaptable to simulations of the scour around tripods in random waves.
- (2) Due to the blockage effects of the main column and structural elements, there are enhanced flow accelerations underneath the main column and the lower diagonal braces, which increases the turbulence intensity and seabed shear stress, leading to more particles being mobilized and transported and thus resulting in more severe scour at the site.
- (3) The revised stochastic model shows that the best agreement with the numerical and experimental results occurs when $n = 20$, but additional experimental data and numerical results are needed to verify the adaptation of the revised stochastic model for larger KC conditions ($KC_{rms,a} > 4$).

Author Contributions: Conceptualization, H.L.; Data curation, R.H. and D.C.; Formal analysis, X.W. and H.L.; Funding acquisition, X.W.; Writing—original draft, R.H. and D.C.; Writing—review and editing, X.W. and H.L. The final manuscript has been approved by all the authors. All authors have read and agreed to the published version of the manuscript.

Funding: This research was funded by the Fundamental Research Funds for the Central Universities (grant number 202061027) and the National Natural Science Foundation of China (grant number 41572247).

Institutional Review Board Statement: Not applicable.

Informed Consent Statement: Not applicable.

Data Availability Statement: The data presented in this study are available from the corresponding author upon request.

Conflicts of Interest: The authors declare no conflict of interest.

References

1. Fazeres-Ferradosa, T.; Rosa-Santos, P.; Taveira-Pinto, F.; Vanem, E.; Carvalho, H.; Correia, J.A.F.D.O. Advanced research on offshore structures and foundation design: Part 1. In *Proceedings of the Institution of Civil Engineers-Maritime Engineering*, 19 December 2019; Thomas Telford Ltd.: London, UK, 2019. [\[CrossRef\]](#)
2. Fazeres-Ferradosa, T.; Rosa-Santos, P.; Taveira-Pinto, F.; Pavlou, D.; Gao, F.P.; Carvalho, H.; Oliveira-Pinto, S. Advanced research on offshore structures and foundation design: Part 2. In *Proceedings of the Institution of Civil Engineers-Maritime Engineering*, 23 December 2020; Thomas Telford Ltd.: London, UK, 2020. [\[CrossRef\]](#)
3. Stahlmann, A. Experimental and Numerical Modeling of Scour at Foundation Structures for Offshore Wind Turbines. Ph.D. Thesis, Franzius-Institute for Hydraulic, Estuarine and Coastal Engineering, Leibniz Universität Hannover, Hannover, Germany, 2013.
4. Yuan, C.G.; Melville, B.W.; Adams, K.N. Scour at wind turbine tripod foundation under steady flow. *Ocean Eng.* **2017**, *141*, 277–282. [\[CrossRef\]](#)
5. Yamini, O.A.; Mousavi, S.H.; Kavianpour, M.R.; Movahedi, A. Numerical modeling of sediment scouring phenomenon around the offshore wind turbine pile in marine environment. *Environ. Earth Sci.* **2018**, *77*, 776. [\[CrossRef\]](#)
6. Hu, R.; Wang, X.; Liu, H.; Lu, Y. Experimental study of local scour around tripod foundation in combined collinear waves-current conditions. *J. Mar. Sci. Eng.* **2021**, *9*, 1373. [\[CrossRef\]](#)
7. Sumer, B.M.; Fredsøe, J. Scour around Pile in Combined Waves and Current. *J. Hydraul. Eng.* **2001**, *127*, 403–411. [\[CrossRef\]](#)
8. Petersen, T.U.; Sumer, B.M.; Fredsøe, J. Time scale of scour around a pile in combined waves and current. In *Proceedings of the 6th International Conference on Scour and Erosion*, Paris, France, 27–31 August 2012.

9. Corvaro, S.; Marini, F.; Mancinelli, A.; Lorenzoni, C.; Brocchini, M. Hydro- and morpho-dynamics induced by a vertical slender pile under regular and random waves. *J. Waterw. Port Coast. Ocean Eng.* **2018**, *144*, 04018018. [[CrossRef](#)]
10. Li, H.; Liu, H.; Liu, S. Dynamic analysis of umbrella suction anchor foundation embedded in seabed for offshore wind turbines. *Geomech. Energy Environ.* **2017**, *10*, 12–20. [[CrossRef](#)]
11. Xu, X.B.; Xu, G.H.; Ren, Y.P.; Liu, Z.Q.; Chen, C.Y. Horizontal normal force on buried rigid pipelines in fluctuant liquefied silty soil. *J. Ocean U. China* **2019**, *18*, 1–8. [[CrossRef](#)]
12. Wu, M.; De Vos, L.; Chavez, C.E.A.; Stratigaki, V.; Fazerer-Ferradosa, T.; Rosa-Santos, P.; Taveira-Pinto, F.; Troch, P. Large scale experimental study of the scour protection damage around a monopile foundation under combined wave and current conditions. *J. Mar. Sci. Eng.* **2020**, *8*, 417. [[CrossRef](#)]
13. Ren, Y.P.; Zeng, Y.; Xu, X.B.; Xu, G.H. Sedimentary changes of a sand layer in liquefied silts. *J. Ocean U. China* **2021**, *20*, 1046–1054. [[CrossRef](#)]
14. Sumer, B.M.; Fredsøe, J.; Christiansen, N. Scour around vertical pile in waves. *J. Waterw. Port Coast. Ocean Eng.* **1992**, *118*, 15–31. [[CrossRef](#)]
15. Sumer, B.M.; Christiansen, N.; Fredsøe, J. The horseshoe vortex and vortex shedding around a vertical wall-mounted cylinder exposed to waves. *J. Fluid Mech.* **1997**, *332*, 41–70. [[CrossRef](#)]
16. Larsen, B.E.; Fuhrman, D.R.; Baykal, C.; Sumer, B.M. Tsunami-induced scour around monopile foundations. *Coast. Eng.* **2017**, *129*, 36–49. [[CrossRef](#)]
17. Umeda, S. Scour regime and scour depth around a pile in waves. *J. Coastal Res.* **2011**, *64*, 845–849.
18. Umeda, S. Scour process around monopiles during various phases of sea storms. *J. Coastal Res.* **2013**, *165*, 1599–1604. [[CrossRef](#)]
19. Yu, T.; Zhang, Y.; Zhang, S.; Shi, Z.; Chen, X.; Xu, Y.; Tang, Y. Experimental study on scour around a composite bucket foundation due to waves and current. *Ocean Eng.* **2019**, *189*, 106302. [[CrossRef](#)]
20. Jalal H, K.; Hassan W, H. Effect of bridge pier shape on depth of scour. In Proceedings of the 3rd International Conference on Engineering Sciences, Gowa, Indonesia, 24–25 September 2019.
21. Hassan W, H.; Jalal H, K. Prediction of the depth of local scouring at a bridge pier using a gene expression programming method. *SN Appl. Sci.* **2021**, *3*, 159. [[CrossRef](#)]
22. Welzel, M.; Schendel, A.; Goseberg, N.; Hildebrandt, A.; Schlurmann, T. Influence of Structural Elements on the Spatial Sediment Displacement around a Jacket-Type Offshore Foundation. *Water* **2020**, *12*, 1651. [[CrossRef](#)]
23. Welzel, M.; Schendel, A.; Hildebrandt, A.; Schlurmann, T. Scour development around a jacket structure in combined waves and current conditions compared to monopile foundations. *Coast. Eng.* **2019**, *152*, 103515. [[CrossRef](#)]
24. Hassan W, H.; Hussein H, H.; Alshammari M, H. Evaluation of gene expression programming and artificial neural networks in PyTorch for the prediction of local scour depth around a bridge pier. *Res. Eng.* **2022**, *13*, 100353. [[CrossRef](#)]
25. DNV. *Design of Offshore Wind Turbine Structures. Offshore Standard DNV-OSJ101*; Det Norske Veritas AS: Berum, Norway, 2013.
26. Yakhot, V.; Orszag, S.A. Renormalization group analysis of turbulence. I. Basic theory. *J. Comput. Sci.* **1986**, *1*, 3–51. [[CrossRef](#)]
27. Yakhot, V.; Smith, L.M. The renormalization group, the e-expansion and derivation of turbulence models. *J. Comput. Sci.* **1992**, *7*, 35–61. [[CrossRef](#)]
28. Mastbergen, D.R.; Berg, J.V.D. Breaching in fine sands and the generation of sustained turbidity currents in submarine canyons. *Sedimentology* **2003**, *50*, 625–637. [[CrossRef](#)]
29. Soulsby, R. *Dynamics of Marine Sands*; Thomas Telford Ltd.: London, UK, 1998.
30. Van Rijn, L.C. Sediment transport, Part I: Bed load transport. *J. Hydraul. Eng.* **1984**, *110*, 1431–1456. [[CrossRef](#)]
31. Yu, Y.X.; Liu, S.X. *Random Wave and Its Applications to Engineering*, 4th ed.; Dalian University of Technology Press: Dalian, China, 2011.
32. Pang, A.L.J.; Skote, M.; Lim, S.Y.; Gullman-Strand, J.; Morgan, N. A numerical approach for determining equilibrium scour depth around a mono-pile due to steady currents. *Appl. Ocean Res.* **2016**, *57*, 114–124. [[CrossRef](#)]
33. Schendel, A.; Welzel, M.; Schlurmann, T.; Hsu, T.W. Scour around a monopile induced by directionally spread irregular waves in combination with oblique currents. *Coast. Eng.* **2020**, *161*, 103751. [[CrossRef](#)]
34. Melville, B.W.; Chiew, Y.M. Time scale for local scour in bridge piers. *J. Hydraul. Eng.* **1999**, *125*, 59–65. [[CrossRef](#)]
35. Yang, L.P.; Shi, B.; Guo, Y.K.; Wen, X.Y. Calculation and experiment on scour depth for submarine pipeline with a spoiler. *Ocean Eng.* **2012**, *55*, 191–198. [[CrossRef](#)]
36. Yang, L.P.; Shi, B.; Guo, Y.K.; Zhang, L.X.; Zhang, J.S.; Han, Y. Scour protection of submarine pipelines using rubber plates underneath the pipes. *Ocean Eng.* **2014**, *84*, 176–182. [[CrossRef](#)]
37. Fazerer-Ferradosa, T.; Chambel, J.; Taveira-Pinto, F.; Rosa-Santos, P.; Taveira-Pinto, F.V.C.; Giannini, G.; Haerens, P. Scour protections for offshore foundations of marine energy harvesting technologies: A review. *J. Mar. Sci. Eng.* **2021**, *9*, 297. [[CrossRef](#)]
38. Myrhaug, D.; Rue, H. Scour below pipelines and around vertical piles in random waves. *Coast. Eng.* **2003**, *48*, 227–242. [[CrossRef](#)]